

Mechanical testing of microelectrode encapsulations used for neural interfaces

Ben Rees¹ and Mohammad Mundiwala²

¹ Combustion Diagnostics Laboratory

² Reliability Engineering and Informatics Laboratory

Keywords: neural interface, mechanical testing, mems

Abstract. This study investigates the mechanical properties of flexible substrate materials and thin-film coatings for soft neural interface applications. Tensile testing of polyimide (PI), PDMS, and kirigami-PI was conducted. PI exhibited the highest modulus and PDMS demonstrated maximum elongation, while kirigami PI provided intermediate properties. Additionally, bi-layer films consisting of silicon carbide (SiC) coatings on PI substrates were analyzed to extract coating modulus. Cracking analysis of SiC thin films of varying thickness, under tensile strain was performed to characterize critical stress-transfer length, interfacial shear strength, and critical energy release rate. Finally, a comparison with MMT nanoclay-PVA nanocomposite films on PET substrates was included to emphasize the impacts of coating on crack-evolution. This work provides insight into the experimental methodologies used to characterize the mechanical properties of thin-films.

1 Introduction

Many modern solutions to Parkinson's disease, epilepsy, spinal cord injury and depression are built on our ability to communicate with the nervous system. Among many design requirements, implantable medical devices (IMDs) must be able to flex and stretch as their environment demands, which is at odds with the brittle and rigid nature inherent to most electronics today. Two distinct approaches may be characterized in the pursuit of more flexible and stretchable electronic devices: material optimization and structural optimization.

The former involves tailoring the mechanical properties of the high-performance encapsulation materials or substrates to which they are adhered to allow for more flexibility while preserving desirable characteristics, such as moisture protection. Even in cases with brittle encapsulation material selection, high-fidelity quantification of the mechanical limits of the material are vital in order to ensure its survival in an applicable environment. Material properties such as the elastic modulus, crack-onset strain, and interfacial adhesion as measured in tensile testing (see Figure 2) are all requisite to ensuring device performance.

The latter option involves optimizing the macro-structure of a locally rigid or brittle material such that the overall structure exhibits stretchable behavior. A powerful example of this is that of Kirigami (shown in Figure 1), where cuts made into a material encourage coordinated flexing in selected areas in such a way that the overall material can elongate. Quantifying by how much a particular strategic structural patterning improves the effective mechanical properties while ensuring local cracking/straining does not exceed damage thresholds gives a clear idea of a particular design's merit.

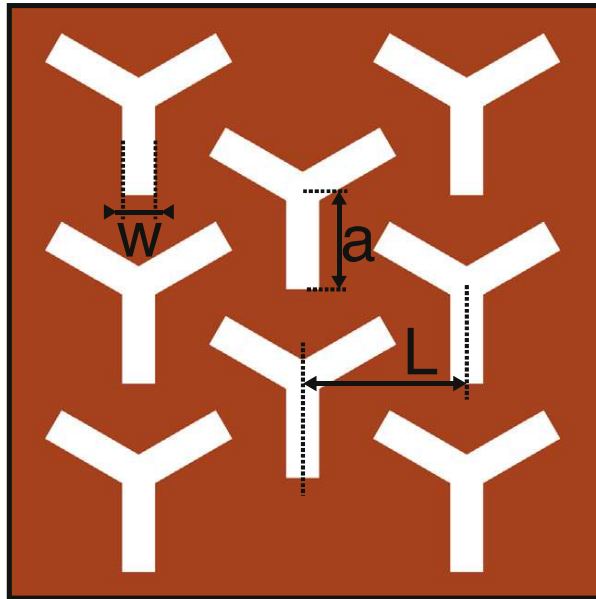


Figure 1: Kirigami pattern used [1], where $w = 0.85$ mm, $a = 2.995$ mm, and $L = 4.28$ mm.

The objective of this lab is to experimentally investigate and compare examples of the two strategies for achieving material compliance. First, in-situ tensile testing is used to characterize the material properties of a brittle encapsulation film (SiC) on a flexible substrate (PI) at varying thicknesses. Second, the effective mechanical properties of a kirigami-patterned substrate are quantified and compared to its bulk counterpart.

2 Data and Methods

2.1 Sample preparation

Three substrate materials were tested: polyimide (PI), polydimethylsiloxane (PDMS), and kirigami PI. Bilayer samples consisting of silicon carbide (SiC) coatings with thicknesses of 500 nm, 1 μ m, and 2 μ m were deposited on PI substrates for fracture analysis. Sample dimensions (width, thickness, and length) were measured with calipers and recorded for stress-strain calculations. Extension and force values were collected using software (DAQ system).

2.2 Kirigami width

The kirigami pattern used in this work is shown by Fig. 1, where the ratio a/L is 0.7. While the full width of the sample is 20 mm, the cutout pattern-widths must be subtracted for a more accurate cross-sectional area calculation. The cutout widths are variable along the length, so an average width is determined by sampling different points and taking the mean. We estimated the effective sample width across four different points and report the average in Table 1.

2.3 Tensile Testing

Uniaxial tensile tests were conducted until failure while force and extension were recorded continuously. The setup shown by Figures 2a and 2b was used for all three materials in this study.

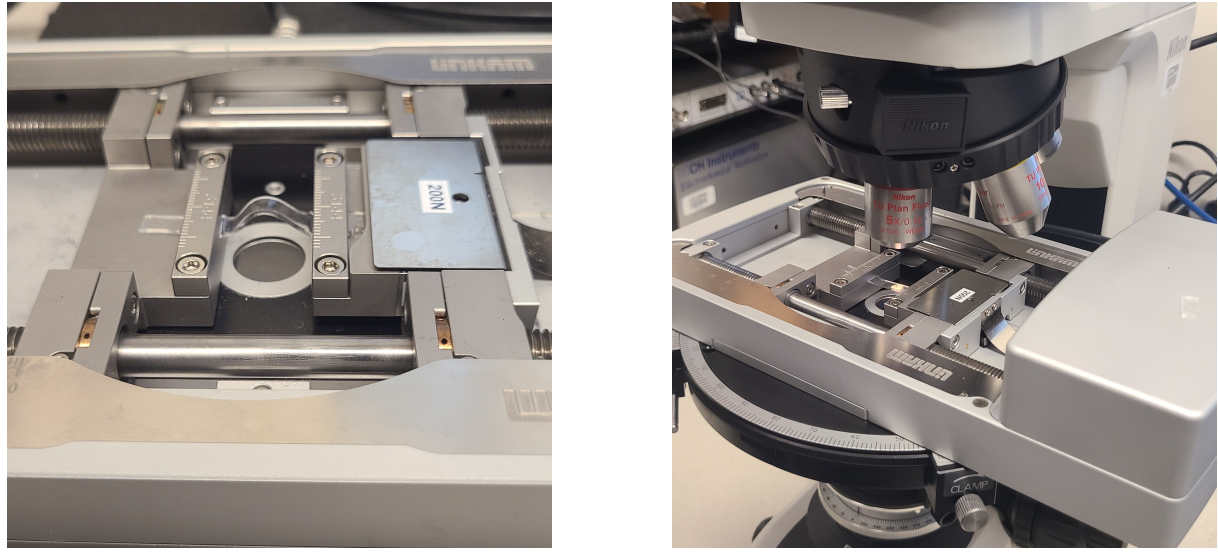


Figure 2: Microscopes and tensile tester used.

Engineering strain and stress were computed as

$$\epsilon = \frac{\Delta L}{L_0} \quad (1)$$

and

$$\sigma = \frac{F}{A_0}, \quad (2)$$

respectively. The elastic modulus E was obtained from the linear region of the stress-strain curve using least-squares fitting, up until a qualitatively selected yield point. Tensile strength and elongation limit were calculated as the maximum stress and strain before failure, respectively. Toughness was determined as the area under the stress-strain curve, using the trapezoid numerical approximation.

2.4 SiC modulus estimation

For SiC-PI bilayers, the coating modulus was calculated using the rule of mixtures. We assume uniform strain for the substrate and coating which is defined by

$$E_{\text{composite}} = \frac{E_1 t_1 + E_2 t_2}{t_1 + t_2}, \quad (3)$$

where $E_{\text{composite}}$, E_1 , E_2 , t_1 , t_2 are the composite, substrate, and coating moduli and their respective thicknesses. The total thickness $t_1 + t_2$ is the thickness of the bilayer thin-film. We estimate the modulus of the encapsulation coating by using the calculated PI modulus from the tensile testing experiments. For these tests, the thicknesses of the coating and substrate were given (not measured) and are included in Table 1.

2.5 Cracking Analysis

In-situ tensile videos were used to identify crack initiation and propagation for the $2 \mu\text{m}$ SiC coated sample. Crack onset strain (COS) ϵ_c corresponded to the strain induced at the onset of the

first visible crack in the in situ microscopy video. At saturation (Stage III), total cracks within the field of view were counted manually to compute the saturated crack density CD_{sat} , given by

$$CD_{\text{sat}} = \frac{N_{\text{cracks}}}{L_{\text{objective}}}, \quad (4)$$

where N_{cracks} and $L_{\text{objective}}$ are the number of cracks counted and the width in mm of the objective view of the microscope.

Screenshots are taken at 0% strain, crack initiation (Stage I), multiplication (Stage II), and saturation (Stage III), completely qualitatively, and are shown in Figure 5.

2.5.1 Critical stress-transfer length

The critical stress-transfer length l_c was determined using

$$l_c = \frac{1}{2 CD_{\text{sat}}} \quad (5)$$

Interfacial shear strength

The interfacial shear strength (IFSS) was estimated using the shear lag model [2]

$$\tau = \frac{E_2 t_2 \epsilon_c}{l_c} \quad (6)$$

where τ represents IFSS. As used in Eq. (3), E_2 and t_2 simply represent the coating modulus and thickness.

Critical energy release rate

The fracture energy G_c was computed as

$$G_c = \frac{E_2 \epsilon_c^2 t_2}{2} \quad (7)$$

where G_c quantifies how much energy per unit area is needed to create a new crack. For this study, lower values of G_c indicate a more brittle and poorly bonded coating, allowing for cracks to spread more easily.

3 Results and Discussions

3.1 Mechanical testing results

The three different materials have entirely different stiffness profiles, shown by Fig. 3, where the stress ranges are different magnitudes. PDMS had the lowest modulus, 0.48 MPa, and the highest elongation, 50%. Therefore, PDMS has the best stretchability but the poorest load-bearing capability. It should be noted that the elongation is much lower than expected, due to a experimental mistake made during the tensile test. The material broke prematurely, right at the fastening point which may indicate an erroneous trial. The PI showed the highest stiffness and tensile strength, 9.2 GPa and 456 MPa, making it the most durable material, at the cost of its flexibility. The kirigami PI lowered the modulus compared to PI alone to 108 MPa, while slightly

Table 1: Data collection results used for stress-strain calculations, where w , t , l_i , and l_f represent width, thickness, initial length, and final length.

Sample Name	w (mm)	t (μm)	l_i (mm)	l_f (μm)
Polyimide	5.18	15.0	19.00	53.8
PI Kirigami	12.20	25.4	23.79	4838
PDMS	5.6	1024.50	22.38	3588.7
SiC 2 μm on 15 μm PI (N0018-2)	4.97	17.0	21.20	46.1
SiC 1 μm on 15 μm PI (NM5-1)	4.86	16.0	21.40	31.7

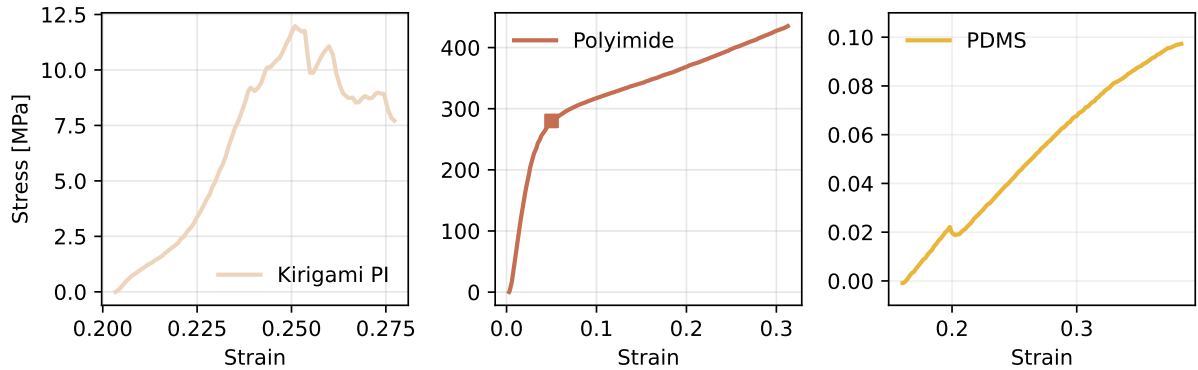


Figure 3: Stress-strain curves for three distinct material substrates

increasing the elongation limit 3% to 40%. This validates the utility of the kirigami structure since it was successfully able to enhance the stretchability, only using structural optimization. Clear trends can be found across the different properties shown by Table 2. For instance, from PI to kirigami to PDMS, the toughness decreases by orders of magnitude, which emphasizes the stiffness flexibility trade-off.

3.2 SiC coating

SiC coating can be useful moisture barrier to the polyimide substrate but will naturally increase the stiffness and brittle nature of the encapsulation. Table 3 shows the modulus values calculated for the bi-layer films. SiC coatings increased the apparent modulus compared to just PI. We can see this trend visually in Fig. 4, particularly to the left of the faint dashed line, where all of the materials are within their elastic regime. We notice the slope increases with the 1 μm coating and even more so with the 2 μm coating.

The calculated SiC coating modulus values (19 - 42 GPa) using the rule of mixtures assumption is an order of magnitude lower than the expected. Possible reason for this are detailed in Section

Table 2: Mechanical properties of three different substrates and encapsulations

Sample	Young's modulus (MPa)	Elongation limit (%)	Toughness (MJ m^{-3})	Tensile strength (MPa)
Polyimide	9242.0	37.6	119.6	456.2
Kirigami	108.4	40.3	0.235	4.91
PDMS	0.48	50.0	0.012	0.097

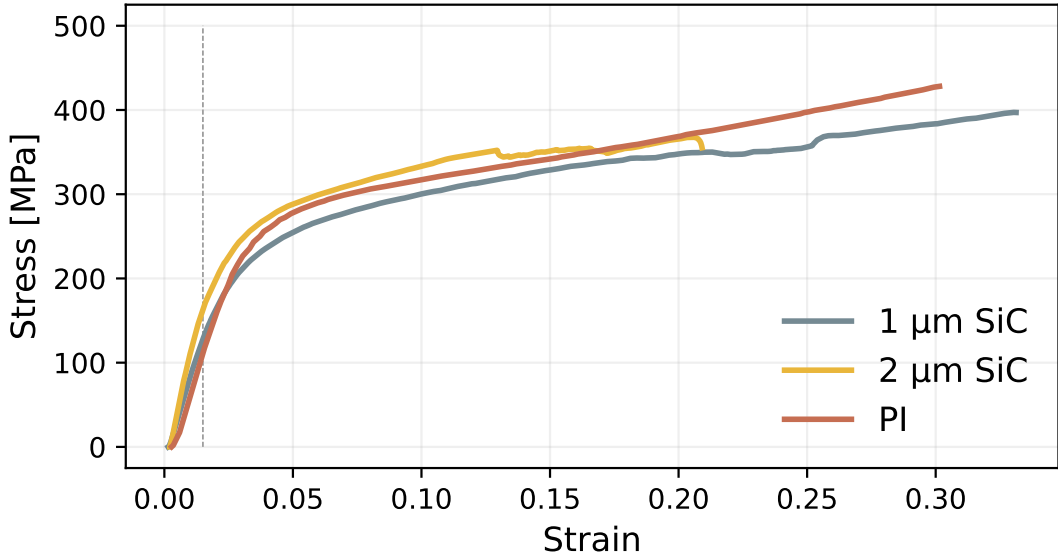


Figure 4: Stress-strain profiles for the different SiC coatings compared against the bulk PI substrate. The faint dashed line signifies the 0.5% strain threshold used for the linear regression.

Table 3: Modulus values for bilayer tensile testing. Apparent modulus refers to the modulus for the entire composite ($E_{\text{composite}}$) and Coating modulus refers to the inferred modulus for SiC using the rule of mixtures defined by Eq. (3)

Material	Apparent modulus (GPa)	Coating modulus (GPa)
SiC 2 μm on PI (N0018-2)	13.11	42.12
SiC 1 μm on PI (NM5-1)	9.86	19.08
Expected [3]	-	435 - 450

3.4. Although the results lack accuracy, we can still extract some valid conclusions based on the trends. Namely, that stiffer coatings improve barrier properties while reducing material compliance which provides designers with an effective knob to tune the material properties of the encapsulation.

3.3 Cracking assessment

A qualitative cracking assessment was completed for the 2 μm SiC coating to calculate CD_{sat} and COS. Using these values, and those provided to us by the instructor, l_c , τ , and G_c were determined and are reported in Table 4. The manually determined crack data (2 μm) generally does match the expected trend. As the coating thickness increases, we notice the materials becomes more brittle and the number of cracks at saturation reduce by approximately 50%. Similarly, the crack on-set strain and the interfacial shear strength decrease with increased coating thickness. Interestingly, and the fracture energy G_c for the 500 nm coating is greater than the 1000 nm coating, yet lower than the 2000 nm coating. Reasons for this non-monotonic behavior and larger limitations in this analysis are detailed in Section 3.4.

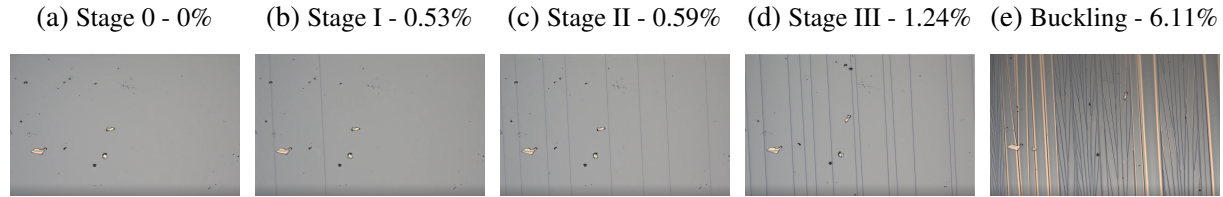


Figure 5: Stages of crack formation as tracked with in-situ microscopy at various strain percentages.

Table 4: Cracking data from SiC coating, 2000 nm sample values determined using qualitative video analysis

t (nm)	CD_{sat} ($\frac{\text{Cracks}}{\text{mm}}$)	COS (%)	l_c (mm)	τ (MPa)	G_c (mJ m^{-2})
500	90.259	0.8965	0.0055	34.09	0.846
1000	38.038	0.6002	0.0131	19.23	0.759
2000	16.256	0.5282	0.0308	14.46	1.175

3.3.1 MMT-PVA

A supplementary experiment was also conducted to assess the cracking of a 50-50 MMT-PVA substrate for comparison with SiC coating on PI. In Fig. 6 the chronological stages of cracking are shown, although it was noticeably more difficult to qualitatively discern these, as compared to Fig. 5. As soon as cracking began, a very short period of time passed before the entire sample was saturated. Note that the strain values are neglected because the original sample length is unknown.

The crack style is notably distinct from the SiC coating; the cracks seen are not clean, straight, and parallel. Instead they are “squiggly,” disconnected, and generally more chaotic. This behavior aligns with what would be expected from a nanocomposite “brick-and-mortar” structured material. Cracks are forced to be deflected and wind around the MMT platelets. This is the primary mechanism for MMT-PVA’s improved toughness and reduced brittleness as compared to the SiC coatings. The comparison of MMT-PVA with SiC-PI helps to highlight the importance of controlled crack propagation for different material coatings.

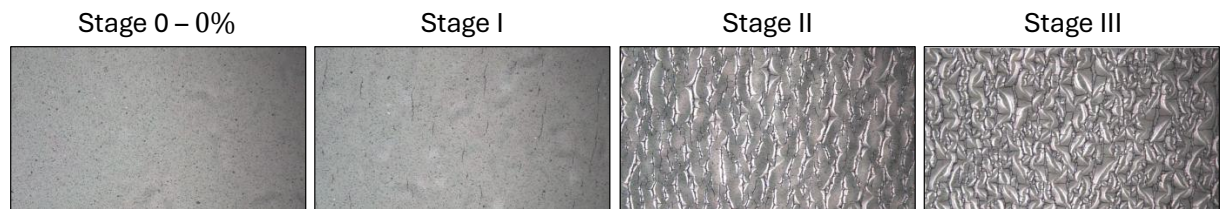


Figure 6: Cracking stages for 50-50 MMT-PVA substrate

3.4 Discussion

The testing framework provided is adequate to show a measurable difference between the different substrates. However, there is strong evidence that the results lack accuracy. Minute

recording errors in the experiments are highly consequential, as shown by the significantly different Young's modulus values calculated for the same material.

The modulus value calculated for SiC coating on the bilayer film was well below the literature range of 435-450 GPa. The most likely cause of this is propagation of uncertainty in the overall and substrate moduli and thickness products, as these values are very large compared to the product of the film modulus and thickness (stiffness). This results in very low resolution in solving for the film properties. Nominal thicknesses were used instead of investigated profiles, which opens the door to manufacturing uncertainty to influence the calculated film modulus as well. Less likely, but also possibly influencing our results, is the influence of the assumption that the SiC film is a continuous and perfect layer that contributes its full stiffness. As a brittle material, it is most likely that the film already contained a network of micro-cracks before the onset of the experiment due to residual stress during the deposition process or material handling. Finally, and least probably the cause of the inaccuracy, is the possibility of the large temperature excursions of the deposition process influencing the substrate properties, making it more compliant. All of these factors in accordance might explain the inaccuracy of our calculated values compared to those reported in more rigorous literature studies.

The cracking assessment could certainly benefit from higher temporal resolution and synchronization between the tensile testing data and microscopy video analysis. The video frame rate is lower than the tensile testing sampling rate and relies on user readiness to select the correct frame from which to interpret the strain data at that cracking stage. Imprecision from this procedure is furthered by the misalignment of the video frames with the tensile testing data; the nearest strain to the selected video frame must be used, which adds uncertainty to the order of $\pm 0.05\mu\text{m}$. Additionally, the unexpected trend in the fracture energy might partially be attributed to the interface adhesion; the system can fail both by cracking and by interfacial delamination. The perfect adhesion implicit to the fracture energy model does not account for the higher elastic energy in thicker films which can disproportionately drive crack tip delamination.

4 Conclusion

In this report we demonstrated a framework to characterize the mechanical properties and fracture mechanics of different material thin-films. The reported results were reasonable and allow us to make conclusions that are consistent with literature. The PDMS sample was the least stiff, the PI was the most stiff, and the kirigami served its purpose by helping to strike a balance between the mechanical properties of both. The assumption used to determine the modulus for the SiC coatings were not validated by the results from this work, but would require further investigation in order to entirely invalidate the approach. The results would be more conclusive with more trials for each material's tensile test, with higher temporal resolution microscopy video-frame analysis, and with video and tensile sampling synchronization. Since the calculated values relied on accurate strain measurements, improving the precision of those results would support for a more rigorous methodology. Nevertheless, the methods used in this work show a valid means to characterize many useful properties of thin-films used for flexible electronics, especially for rapid design development.

Availability of data and code

Our code is available at the following URL: <https://github.com/mohammadmundiwala/Flexible-Electronics/tree/main/lab-3>.

References

- [1] Nicolas Vachicouras, Christina M Tringides, Philippe B Campiche, and Stéphanie P Lacour. Engineering reversible elasticity in ductile and brittle thin films supported by a plastic foil. *Extreme Mechanics Letters*, 15:63–69, 2017.
- [2] Ha L Cox. The elasticity and strength of paper and other fibrous materials. *British journal of applied physics*, 3(3):72, 1952.
- [3] SGL Carbon. Sigrafine sic coatings. <https://www.sglcarbon.com/en/markets-solutions/material/sigrafine-sic-coating/>, 2025. Accessed 22 October 2025.